Ecological Informatics 67 (2022) 101493

Contents lists available at ScienceDirect

Ecological Informatics

journal homepage: www.elsevier.com/locate/ecolinf

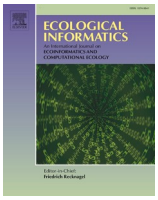

Determination of urban pollution islands by using remote sensing technology in Moscow, Russia

Natalia Bakaeva, Minh Tuan Le *

Department of Urban Planning, NRU MGSU, Moscow, Russia

ARTICLE INFO

Keywords:
Air pollution
Aerosol optical thickness
Geographic information system
Particulate matter
Remote sensing
Urban heat island

ABSTRACT

Pollution of the atmosphere with harmful substances is currently the most dangerous form of degradation of the natural environment in Russia. The peculiarities of the environmental situation and the emerging environmental problems in some areas of the Russian Federation are caused by local natural conditions and the nature of the impacts from industries, transport, utilities, and agriculture (the specifics of enterprises, their capacity, location, technologies used). As a rule, the magnitude of air pollution depends on the degree of urbanization and anthropogenic transformation of the territory and climatic conditions that determine the potential for atmospheric pollution. During high-temperature technological processes, the smallest aerosol particles (0.5..0.10 μm) formed, poorly captured by gas purification plants, and can migrate in the atmosphere for considerable distances. Larger particles (2.5 μm and above) are formed due to the mechanical decomposition of solid particles and enter the atmosphere due to wind erosion, the dusting of dirt roads, the erasure of vehicle tires. The particles suspended with a diameter of not more than 2.5 μm (PMX) are the most destructive to health since they penetrate and get deposited deep into human lungs. These microns, present in a suspended state in the air, consist of a complex mixture of large and small, solid and liquid particles, of both inorganic and organic substances. The boundary between the two fractions is usually particles with a diameter of 2.5 μm (PM2.5). This study sought to build a model for determining fine dust PM2.5 in the Moscow air environment using Landsat 8 OLI satellite image channels and data on the concentrations of fine dust PM2.5 obtained by weather stations in the city. In addition, a correlation analysis was carried out to determine a regression model for studying the dispersion of fine dust in the city. The results obtained are presented on a map of the concentration of fine dust PM2.5 in Moscow, supporting management decisions and decision-making on environmental policy in urban planning.

1. Introduction

According to Imhoff et al., Intensive changes in human settlement, energy use, consumption of natural resources, transportation, industry, and population growth patterns manifested through Urban heat island (UHI) and urban pollution island (UPI) (2010).

An urban heat island is a change in heat balance in urban spaces compared to nearby rural areas due to changes in heat transfer and the amount of movement between the Earth's surface and the atmosphere in terms of heat storage, the separation between explicit and latent heat flows (Bowen ratio), friction resistance and the balance between natural and anthropogenic emissions (Vailshery et al., 2013).

The "urban pollution island" was a term recently introduced (Crutzen, 2004) to denote the beginning of temporal and spatial changes in the concentration of pollutants attributed to the presence of typical urban features and activities. The differences between suburban, metropolitan areas and rural regions determine the intensity of urban pollution by analogy with the intensity of the urban heat island. UHI and air pollution are far from independent phenomena, to the extent that where urban heat islands exist, urban pollution islands most likely coexist (Crutzen, 2004). High temperatures accelerate specific chemical cycles of the atmosphere, most of which lead to an increase in surface (tropospheric) ozone formation, an increase in emissions of biogenic hydrocarbons (Elsayed, 2012). Moreover, conditionally, it leads to the release of exhaust gas heat into the urban air, thereby fueling the strengthening of the UHI in an ever-increasing spiral. Turbulent mixing is stimulated by warmer air, promoting the spread of primary pollutants to higher layers of the atmosphere (Sarrat et al., 2006).

The rapid pace of industrialization, the constant population increase, the upsurge in the number of vehicles and traffic density, the decrease in

* Corresponding author.
E-mail address: architect290587@gmail.com (M.T. Le).

https://doi.org/10.1016/j.ecoinf.2021.101493
Received 18 September 2021; Received in revised form 9 November 2021; Accepted 20 November 2021
Available online 23 November 2021

green areas, the presence of industries in Moscow lead to significant environmental pollution. Urbanization causes substantial changes in the atmospheric air, increased pollutants concentrations, and fine dust particles that pose a severe threat to public health. The World Health Organization (WHO) classifies fine particles with a size of no less than 10 μm (PM10, PM2.5) as priority pollutants entering the atmospheric air according to the level of impact on public health. PM2.5 is particularly dangerous. PM2.5 aerosols can directly penetrate the human lungs through the respiratory tract, thus affecting their health (Raaschou-Nielsen et al., 2013). According to a report by WHO, more than 90% of the world's population inhales large amounts of pollutants every day, leading to an estimated seven million deaths annually. Therefore, an assessment of the concentration of PM2.5 is required, and it becomes a significant problem for human health (Melstrom et al., 2017).

Airborne fine dust particles refer to solid or liquid elements suspended in the air. In addition, they are very heterogeneous both in space and in time and are often observed as smoke, dust, and haze. PM2.5 and PM10 are defined as particles with a diameter of 2.5 μm or less and 10 μm or less, and respectively, these are standard concentrations used by the US Environmental Protection Agency (EPA). Aerosol is defined as the total number of particles suspended in the air with a typical particle radius from 0.05 to 15 μm (Dubovik et al., 2001). Aerosol particles' scattering and absorption of light to poor visibility (Kaufman et al., 1997). Satellite remote sensing of aerosols allows obtaining data on the Aerosol Optical Thickness (AOT) as a quantitative measurement of the content of solid particles in the atmospheric column(Liu et al., 2009). To a certain degree, AOT can be considered an important and the easiest recognized indicator of air pollution and the presence of solid particles in the air.

The most challenging task is to obtain information about the fractions of fine particles from remote measurement data. This is the conversion of optical parameters of aerosol into a mass concentration of PM2.5 (from now on, also referred to as PM2.5). Earlier studies assumed that there were mysterious relations between the aerosol optical thickness (AOT) and PM2.5. A linear regression of AOD – PM2.5 was usually used to represent their correlation (Engel-Cox et al., 2004; Wang and Christopher, 2003). Meanwhile, other studies have proved the presence of a significant nonlinear relationship between AOT and PM2.5 (Hutchison et al., 2005) due to the variety of optical properties of the aerosol with variations in granulometric composition, composition, and shape. Many statistical expressions were developed to describe the AOD – PM2.5 relationship (Paciorek and Liu, 2009).

The sources of suspended particles entering the atmospheric air of Moscow are emissions from industrial enterprises, emissions of motor vehicles (mainly diesel), construction work, fine dust from paved areas of territories, and unpaved soil areas.

The research in this paper is based on a statistical analysis of meteorological measurement data and the observed air pollution at ground stations. Based on these measurements and the spatial distribution of fine dust, air pollutants were estimated using dispersion and interpolation methods. The accuracy of the process depends on the number and location of monitoring stations. The denser the number of measuring stations, the more accurate the results. However, the construction of air monitoring stations is economically costly, so it is impractical. Moreover, urban areas with a characteristic pronounced uneven relief of urban development due to different heights of buildings.

However, data for the entire study area is provided in a continuous network structure of adjacent pixels when using satellite images. Each pixel is similar to a monitoring station, so the number of data measurement points from the satellite is much higher than ground-based measuring stations. The results of the satellite image analysis show the values for each pixel depending on the image resolution and the territory for different observation periods, which is extremely difficult to achieve when setting up ground-based monitoring stations.

Studies worldwide show that multispectral satellite images allow to detection of air pollution in areas of interest. Several studies have shown a conceivable link between satellite data and air pollution (Liaw et al., 2020; Shi et al., 2012; Zhang and Li, 2015). Data from the Landsat 8 OLI satellite has been used since 2013. This study presents the results on the scattering of suspended particles of no more than 2.5 μm in diameter (PM2.5) in the air using experimental satellite images of Landsat 8 OLI in Moscow.

2. Study area

Moscow, located in the center of the East European Plain, between the Oka and Volga Rivers, was chosen to study at an average altitude of 180 m above sea level. The city characterizes by a humid temperate continental climate with a clearly defined seasonality (climatic region IIB according to SP 131.13330.2018). Currently, Moscow covers an area of about 2561 km^2, while the population density in the city is 4956 people/km^2 (2020). According to official data, about 12.6924 million people live in the city (according to unofficial data, about 20 million people). According to Moscow City State Statistics Committee forecasts, by 2030, the population of Moscow is estimated to hit the mark of 13.65 million people. According to mathematical predictions based on the graph's data on the people of the city for 30 years, the population of Moscow may reach 15 million people.

Fig. 1 shows the scheme of the administrative division of Moscow city, indicating the location of the weather stations that provided data for the study.

2.1. Description of the nature of the image obtained by the Landsat 8 satellite in the city of Moscow

The Landsat 8 OLI satellite successfully launched in 2013 with two primary sensors: a ground image receiver (OLI-Operational Land Imager) and a thermal infrared sensor (TIRS-Thermal Infrared Sensor)

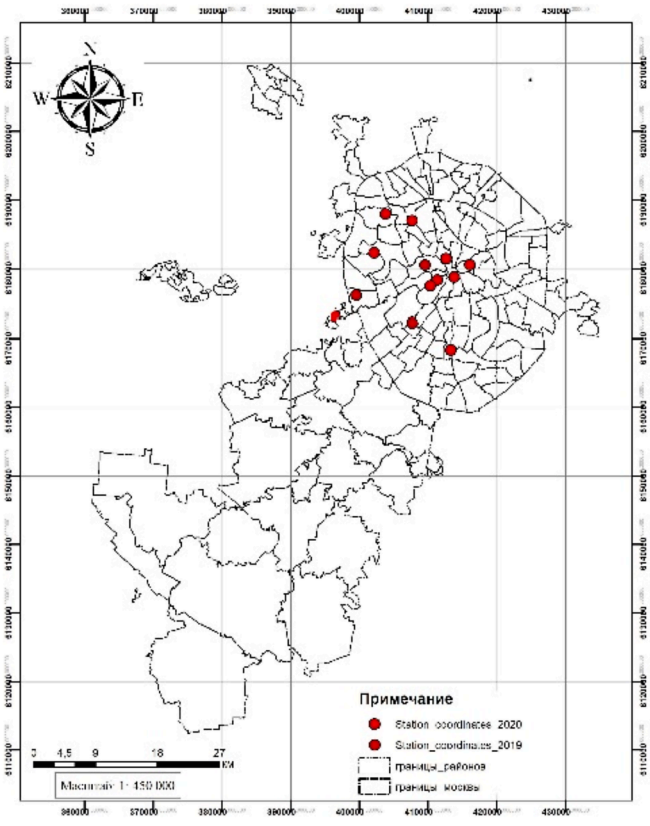

Fig. 1. The scheme of administrative division of the city of Moscow with the location of the weather stations provided data for the study.

(*Landsat 8 (L8)* Data Users Handbook, 2019) (Tables 1, 2.1–2.4).

The image of Landsat 8 OLI used in the study is provided on the website http://landsat.usgs.gov. The image was processed by the provider at level 1 with the image numbers: LC 08_L1TP_179021_2019 06_200828_02_T1 and LC08_L1TP_179022_20190606_20200828_02_T1 on 06.06.2019 LC08_L1TP_178021_20201210_20210312_02_T1 and LC08_L1TP_178022_20201210_20210312_02_T1 on 10.12.2020.

2.2. Data on the concentration of fine PM2.5 particles recorded by CityAir weather stations

2.2.1. Description of the device used for measuring fine particles of PM2.5

Monitoring of the state of dust pollution of the environment with suspended substances PM2.5 and PM10 carries out by dust analyzers. The most widely used dust analyzers are based on a microbalance, radioisotope, and nephelometric, each of which has certain advantages and limitations.

Dust meters using the microbalance method are based on a change in the frequency of natural mechanical vibrations of a glass tube as solid particles deposited on a quartz filter.

Dust meters using the radioisotope method are based on the attenuation of the intensity of ionizing radiation when passing through a layer of matter (thus, its size is also determined).

Dust meters using the nephelometric method are based on the intensity of a monochromatic light beam scattered at an angle of 90° on the size and concentration of particles.

In the framework of the study, the concentration of suspended PM2.5 particles was recorded by the equipment of CityAir, an organization for monitoring air quality, using the CityAir Dust fine meter (no. in the GRSI of the Russian Federation: 75984–19) (Fig. 2), which designs to determine PM2.5 in the air by the nephelometric method (Table 3). When using the CityAir Dust device, the particle sizes are directly determined. This dust analyzer has a feature that allows measurements to carry out without using a selective impactor.

It should note that the nephelometric method is an indirect measurement method that bases on the assumption of the density and size distribution of particles; this is embedded in the algorithm for restoring the mass concentration by the intensity of scattered light incident on the photodetector. The readings of nephelometric dust meters must normalize due to differences in the distribution of suspended substances in the urban air compared with the reference values of aerosols used for calibration.

Moreover, when normalizing PM2.5 values with the CityAir Dust device, various models can be used. Terms used:

A dust analyzer (dust meter) measures the diameter and the counting or mass concentration of suspended substances.

Suspended substances PM2.5 are particles that pass through a selective impactor that provides 50% screening of particles with an aerodynamic diameter of 2.5 μm, and the upper limit of complete screening is 7 μm.

Table 1
Spatial resolution of Landsat 8 OLI and image channels.

Image channels	Wavelength (λ, μm)	Resolution (m)
Channel 1- Coastal aerosol	0.43–0.45	30
Channel 2- Blue	0.45–0.51	30
Channel 3- Green	0.53–0.59	30
Channel 4- Red	0.64–0.67	30
Channel 5- Near Infrared (NIR)	0.85–0.88	30
Channel 6- SWIR 1	1.57–1.65	30
Channel 7- SWIR 1	2.11–2.29	30
Channel 8- Panchromatic	0.50–0.68	15
Channel 9- Cirrus	1.36–1.38	30
Channel 10- Thermal Infrared (TIRS) 1	10.60–11.19	100
Channel 10- Thermal Infrared (TIRS) 2	11.50–12.51	100

2.2.2. Actual data of the concentration values of fine PM2.5 particles recorded by CityAir weather stations

The concentration values of fine PM2.5 particles take from all existing City Air stations in Moscow for 2019. The importance of fine PM2.5 particles used to compare with the results obtained by remote sensing is presented in Tables 4.1 and 4.2 below.

3. Methodology

In this study, the remote sensing method was used to construct a PM2.5 concentration scheme. The research process is divided into the following stages: data collection, image pre-processing, data processing, model selection, and evaluation of the results. All steps of pre-processing and data processing are performed using the ArcGIS and Microsoft Excel programs.

3.1. Pre-processing of images

Image pre-processing performs by converting numeric values (DN-Digital number) into a spectral wavelength or a matter of spectral reflectivity with several levels of radiation correction. First, the numerical values convert to the radiation values at the receiver. Then the spectral radiation at the receiver is converted back into the spectral radiation on the Earth's surface. Finally, after the previous stages, it is necessary to carry out an atmospheric correction to eliminate the influence of atmospheric conditions on the image quality (Fig. 3).

3.2. Conversion of numerical values into spectral radiation values at the peak of the atmosphere (TOA)

Landsat 8 OLI image Data (*Landsat 8 (L8)* Data Users Handbook, 2019) the data of the peak spectral radiation of the atmosphere converted into the following formula:

$$L_\lambda = M_L{}^* Q_{cal} + A_L \quad (1)$$

where L_λ−is the peak spectral radiation of the atmosphere (Watts / (m2 * srad * microns));

M_L−is the coefficient of the change in the radiation coefficient of the image channel by a set of multiples taken in the metadata file (RADIANCE_MULT_BAND_x, where x is the image channel);

A_L−is the coefficient of change in the radiation power of the image channel by cumulative nature, taken in the metadata file (RADIANCE_ADD_BAND_x, where x is the image channel);

3.3. Converting numerical values into reflection in the upper part of the atmosphere

The data from the Landsat 8 OLI image channels are converted to reflection in the upper part of the TOA atmosphere using the regression reflection coefficient provided in the metadata file (MTL file). The following equation is used to convert DN values to TOA reflection for Landsat 8 OLI data (*Landsat 8 (L8)* Data Users Handbook, 2019):

$$\rho\lambda' = M_\rho{}^* Q_{cal} + A_\rho \quad (2)$$

where, $\rho\lambda'$−TOA reflection at the top of the atmosphere without correction for the angle of incidence; M_ρ− coefficient of change in the reflection coefficient of the image channel according to the multiplicity property taken in the metadata data file (REFLECTANCE_MULT_BAND_x, where x is the image channel); A_ρ−coefficient of change in the reflectivity of the image channel by the aggregate character, taken in the metadata data file (REFLECTANCE_ADD_BAND_x, where x is the image channel); Q_{cal}−quantization and standard calibration of the conversion of numerical values of channels.

Table 2.1
Parameters of the image capture date channel (path:179, row: 021) Landsat 8 OLI on 06.06.2019:

Image channels	M_L	A_L	Mp	Ap	$ESUN_\lambda$	Lmax	Lmin
Channel 1	0,012194	−60,96,806	0,00002	−0,1	1971,25	738,14,038	−60,95,587
Channel 2	0,012486	−62,43,204	0,00002	−0,1	2018,59	755,86,475	−62,41,956
Channel 3	0,011506	−57,53,059	0,00002	−0,1	1860,11	696,52,289	−57,51,908
Channel 4	0,0097026	−48,51,304	0,00002	−0,1	1568,55	587,34,735	−48,50,333
Channel 5	0,0059375	−29,68,756	0,00002	−0,1	959,875	359,42,728	−29,68,162
Channel 6	0,0014766	−738,303	0,00002	−0,1	238,712	89,38,629	−738,155
Channel 7	0,00049769	−248,847	0,00002	−0,1	80,4588	30,12,797	−248,798
Channel 8	0,010981	−54,90,341	0,00002	−0,1	1775,17	664,71,552	−54,89,243
Channel 9	0,0023205	−11,60,257	0,00002	−0,1	375,141	140,47,234	−11,60,025

Table 2.2
Parameters of the image capture date channel (path:179, row: 022) Landsat 8 OLI on 06.06.2019.

Image channels	M_L	A_L	Mp	Ap	$ESUN_\lambda$	Lmax	Lmin
Channel 1	0,012194	−60,96,806	0,00002	−0,1	1971,25	738,14,032	−60,95,587
Channel 2	0,012486	−62,43,204	0,00002	−0,1	2018,59	755,86,469	−62,41,955
Channel 3	0,011506	−57,53,059	0,00002	−0,1	1860,11	696,52,283	−57,51,908
Channel 4	0,0097026	−48,51,303	0,00002	−0,1	1568,55	587,34,729	−48,50,333
Channel 5	0,0059375	−29,68,756	0,00002	−0,1	959,875	359,42,725	−29,68,162
Channel 6	0,0014766	−738,303	0,00002	−0,1	238,712	89,38,629	−738,155
Channel 7	0,00049769	−248,847	0,00002	−0,1	80,4588	30,12,796	−248,798
Channel 8	0,010981	−54,90,340	0,00002	−0,1	1775,17	664,71,552	−54,89,242
Channel 9	0,0023205	−11,60,257	0,00002	−0,1	375,141	140,47,232	−11,60,025

Table 2.3
Parameters of the image capture date channel (path:178, row: 021) Landsat 8 OLI on 10.12.2020.

Image channels	M_L	A_L	Mp	Ap	$ESUN_\lambda$	Lmax	Lmin
Channel 1	0,01295	−64,73,693	0,00002	−0,1	1971,25	783,77,002	−64,72,398
Channel 2	0,01326	−66,2914	0,00002	−0,1	2018,59	802,59,003	−66,27,814
Channel 3	0,01222	−61,08696	0,00002	−0,1	1860,11	739,57,983	−61,07475
Channel 4	0,0103	−51,51,197	0,00002	−0,1	1568,55	623,6554	−51,50,167
Channel 5	0,0063	−31,52,276	0,00002	−0,1	959,875	381,646	−31,51,645
Channel 6	0,00157	−783,942	0,00002	−0,1	238,712	94,91,189	−783,785
Channel 7	0,00053	−264,231	0,00002	−0,1	80,4588	31,99,039	−264,178
Channel 8	0,01166	−58,29,737	0,00002	−0,1	1775,17	705,80,627	−58,28,571
Channel 9	0,00246	−12,31,981	0,00002	−0,1	375,141	149,15,591	−12,31,734

Table 2.4
Parameters of the image capture date channel (path:178, row: 022) Landsat 8 OLI on 10.12.2020.

Image channels	M_L	A_L	Mp	Ap	$ESUN_\lambda$	Lmax	Lmin
Channel 1	0,01295	−64.73693	0,00002	−0,1	1971,25	783,77,002	−64,72,398
Channel 2	0,01326	−66.29141	0,00002	−0,1	2018,59	802,59,009	−66,27,815
Channel 3	0,01222	−61.08697	0,00002	−0,1	1860,11	739,5799	−61,07475
Channel 4	0,0103	−51.51197	0,00002	−0,1	1568,55	623,65,546	−51,50,167
Channel 5	0,0063	−31.52276	0,00002	−0,1	959,875	381,64,603	−31,51,645
Channel 6	0,00157	−7.83942	0,00002	−0,1	238,712	94,9119	−783,786
Channel 7	0,00053	−2.64231	0,00002	−0,1	80,4588	31,99,039	−264,178
Channel 8	0,01166	−58.29737	0,00002	−0,1	1775,17	705,80,634	−58,28,571
Channel 9	0,00246	−12.31981	0,00002	−0,1	375,141	149,15,591	−12,31,734

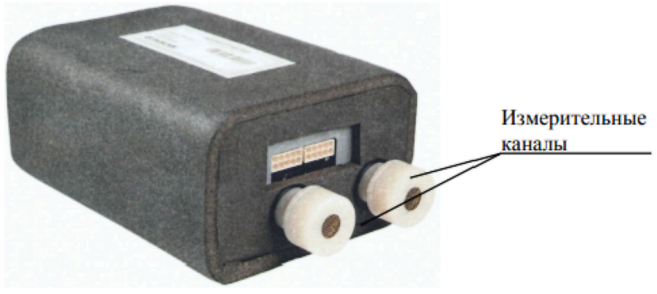

Fig. 2. The appearance of CityAir Dust meters with an indication of measuring channels.

Table 3
Technical characteristics of the City Air Dust analyzer used for fixing PM2.5.

Name of the parameter or characteristic	Value
Electrical power supply parameters:	
AC voltage	от 207 до 253
V - frequency of alternating current	от 49 до 51
Power consumption, V*A, no more	50
Overall dimensions of the dust meter, mm, no more:	
Height-width-length	110,170,300
Weight, kg, no more	1,6
Operating conditions:	
Ambient temperature, °C	от −40 до +50
Relative humidity of the environment, %, no more	98
Atmospheric pressure, kPa	от 84 до 106,7

Table 4.1
Data of PM2.5 concentration values recorded by City Air stations in Moscow using the CityAir Dust meter in the period from 8: 00 to 9: 00, 06.06.2019.

№	Location of the measurement point			PM2.5 sr, μg/m3	PM2.5 sr correct, μg/m3
	Address of the weather station	Latitude	Longitude		
1	Balchug str., 5	55,74,717	37,62,665	0,008	0,003
2	Beregovaya str., 3	55,828,169	37,464,339	0,008	0,003
3	Bolshoy Levshinsky lane, 11	55,74,299	37,58,831	0,007	0,003
4	Kashirsky proezd, 10	55,653,223	37,622,344	0,006	0,002
5	Malaya Dmitrovka str., 18A	55,77,128	37,60,682	0,008	0,003
6	Priorova str., 16к1	55,81,998	37,526,537	0,005	0,005
7	Weather station in Tamansky puffin	55,777,043	37,440,135	0,009	0,004
8	1905 goda str., 7/1	55,7621	37,55,867	0,007	0,003
9	Stroiteley str., 11	55,687,015	37,531,954	0,008	0,003
10	Tolbukhina str., 9к1	55,72,123	37,40,099	0,007	0,003

Table 4.2
Data of PM2.5 concentration values recorded by City Air stations in Moscow using the CityAir Dust meter in the period from 8: 00 to 9: 00, 10.12.2020.

№	Location of the measurement point			PM2.5 sr, μg μg/m3	PM2.5 sr correct, μg/m3
	Address of the weather station	Latitude	Longitude		
1	Balchug str., 5	55,74,717	37,62,665	0,032	0,012
2	Beregovaya str., 3	55,828,169	37,464,339	0,025	0,010
3	Bolshoy Levshinsky lane, 11	55,74,299	37,58,831	0,031	0,012
4	Kashirsky proezd, 10	55,653,223	37,622,344	0,037	0,015
5	Malaya Dmitrovka str., 18A	55,77,128	37,60,682	0,026	0,010
6	Priorova str., 16к1	55,81,998	37,526,537	0,035	0,014
7	1/3 Tamansky puffin street	55,777,043	37,440,135	0,025	0,010
8	Gorokhovsky lane, 4	55,7636	37,66,295	0,027	0,011
9	Pogodinskaya Street, 2	55,73,513	37,57,228	0,030	0,012
10	Zvorykin Street, 1 k2	55,69,353	37,35,213	0,025	0,010

3.4. TOA reflection in the upper part of the atmosphere when adjusting the angle to the sun

$$\rho\lambda = \frac{\rho\lambda'}{cos(\theta_{SZ})} = \frac{\rho\lambda'}{sin(\theta_{SE})} \quad (3)$$

where $\rho\lambda$– reflection in the upper part of the atmosphere (TOA); θ_{SE}– angle to the sun (SUN_ELEVATION); θ_{SZ}–the angle at the top of the sun; $\theta_{SZ} = 90^\circ - \theta_{SE}$.

3.5. Atmospheric correction

To determine the reflection coefficient of the atmosphere, we need to draw the reflection coefficient from the surface. However, when light passes through the atmosphere, it is affected by the scattering and absorption of particles suspended in the atmosphere. Therefore, to improve the results of determining the reflection from the Earth's surface, it is necessary to introduce a correction to the atmosphere.

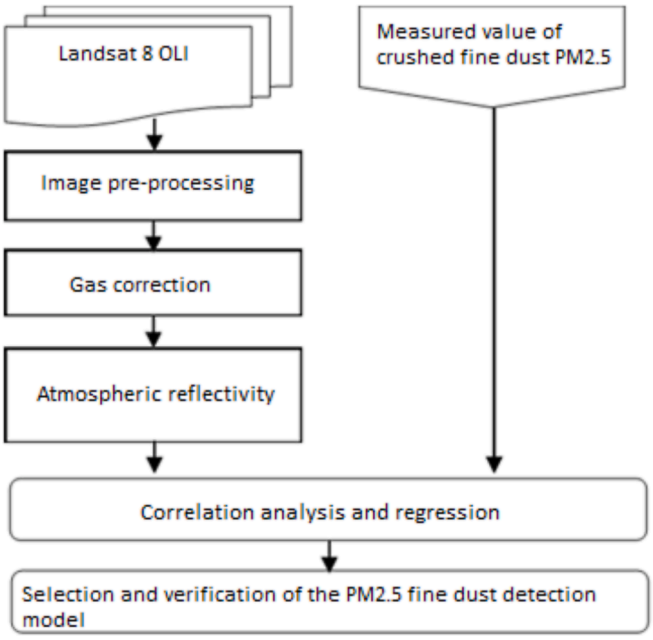

Fig. 3. Scheme of the procedure for determining fine particles of PM2.5 according to the data of the Landsat 8 OLI satellite image and the data of dust measurement in the surface layer of the atmosphere.

The attached Landsat 8 OLI image allows to directly convert the numerical values of the image into a reflection in the upper part of the atmosphere (TOA), thereby continuing to calculate the reflection coefficient on the Earth's surface. According to (Susan Moran et al., 1992), the reflection from the Earth (p) is calculated by the following formula:

$$\rho = \frac{\pi^*(L_\lambda - L_P)^*d^2}{T_v^*\{(ESUN_\lambda^*cos(\theta_{SZ})^*T_Z) + E_{down})\}} \quad (4)$$

where L_P–radiation transmission line; T_v– function transmits radiation through the atmosphere from the Earth's surface to the receiver; T_Z–function transmits radiation through the atmosphere from the sun to the Earth's surface; E_{down}– the spectral radiation propagates to the plane of the object's surface; $ESUN_\lambda$– spectral radiation of the sun on the terrain plane perpendicular to the sun's rays; d– distance from the Earth to the sun.

To correct the atmosphere, the method of subtracting DOS (Dark Object Subtraction) (Chavez, 1996) and determining the transmission line radiation (Sobrino et al., 2004) is used. The DOS method excludes the influence of the atmosphere based on the reflection of objects. This is a simple method based on the obtained reflectivity (TOA) of the image channels themselves. The principle of this method is based on the assumption that some pixels of the satellite image will have zero reflectivity. Therefore, measured values of this object's reflection coefficient in the image result from the scattering of rays in the atmosphere. The DOS method is simple and has particular effectiveness in correcting atmospheric influences like removing haze. The following formula exists for the Landsat 8 OLI image:

$$L_P = L_{min} - 0,01^*\frac{T_V^*\{(ESUN_\lambda^*cos(\theta_{SZ})^*T_Z) + E_{down}\}}{\pi^*d^2} \quad (5)$$

where L_{min}– minimum spectral illumination of the image channel taken in the metadata file (RADIANCE_MINIMUM_BAND_x, where x is the image channel).

The DOS method depends on the parameters T_V, T_Z и E_{down} Moreover,

it is divided into several types (DOS1, DOS2, DOS3, DOS4).

In this study, we used DOS1. The parameters were determined as (Susan Moran et al., 1992) T_V=1; T_Z=1; E_{down}=0. The formula calculates the radiation of the transmission line:

$$L_P = L_{min} - 0,01*\frac{ESUN_\lambda * cos(\theta_{SZ})}{\pi * d^2} \quad (6)$$

Moreover, the reflection from the Earth's surface is calculated using the following formula:

$$\rho = \frac{\pi * (L_\lambda - L_p) * d^2}{ESUN_\lambda * cos(\theta_{SZ})} \quad (7)$$

where $ESUN_\lambda = \pi d^2$ (Radiance_maximum / Reflectance_ maximum) (Bilal et al., 2019), Radiance_maximum и Reflectance_ maximum presented in the Landsat 8 metadata file.

3.6. Preparation of the atmospheric reflection value

The reflection in the upper part of the atmosphere is equal to the sum of the reflection from the Earth and the atmospheric reflection, so the reflection coefficient of the atmosphere is calculated using the formula (Somvanshi et al., 2019).

$$R_{atm} = \rho\lambda - \rho \quad (8)$$

where, R_{atm}– atmospheric reflection; $\rho\lambda$– reflection in the upper part of the atmosphere (TOA); ρ– reflection from the Earth.

The relationship between the aerosol thickness (AOT) and the PM2.5 dust content: Solar energy enters the aerosol layer in the troposphere under the influence of polluted gas molecules and dust particles, is partially reflected in the aerosol layer, and then enters the satellite image receiver. Some of the sun's rays hit an object on the Earth, the surface, and then are reflected in the satellite image receiver. Based on the energy losses in the satellite receiver due to the absorption and scattering of polluting gas molecules and dust particles, the dust content in the air is calculated.

After adjusting the atmosphere, we calculate the reflection in the upper part of the atmosphere (TOA) and the reflection from the surface of the Earth, based on which the reflection coefficient of the atmosphere is calculated. The aerosol optical thickness (AOT) is calculated as follows (Othman et al., 2010):

$$AOT(\lambda) = a_0 R(\lambda) \quad (9)$$

where R (λ) is the reflection function of the atmosphere corresponding to the wave (λ).

Equation (8) is rewritten for the image channels as follows:

$$AOT(\lambda) = a_0 R_{\lambda 1} + a_j R_{\lambda 2} + a_2 R_{\lambda 3} + \cdots \quad (10)$$

where, $R_{\lambda i}$– reflection coefficient of the atmosphere (i = 1, 2 and 3 for satellite wavelengths), and a_j is the algorithmic coefficient (j = 0, 1 and 2) determined experimentally.

The connection between fine dust (PM) and AOT occurs from a pure homogeneous layer containing spherical aerosol particles. The surface concentration is obtained after drying the air sample.

$$PM_x = \frac{4}{3}\pi\rho \int_0^{X/2} r^3 n(r) dr \quad (11)$$

where n (r) describes the granulometric composition under dry conditions, and p is the mass density of the aerosol.

Thus, it was found that the PM content correlates better with direct AOT. Replacing AOT with PM2.5 in equation (9), we get equation (11), and the algorithm for the image channel or wavelength (λ), PM2.5, is simplified by the formula (Lim et al., n.d.; Othman et al., 2010):

$$PM2,5 = a_0 R_{\lambda 1} + a_j R_{\lambda 2} + a_2 R_{\lambda 3} + \cdots \quad (12)$$

where $R_{\lambda i}$– is the reflection coefficient of the atmosphere (i = 1, 2, and 3, corresponding to the wavelength of the satellite), and a_j is the algorithmic coefficient (j = 0, 1 and 2), determined experimentally.

3.7. Determination of the error

The uncertainty is calculated between the estimated dust value from the equation and the actual measured dust value:

$$RMSE = \sqrt{\frac{\sum (P_{calculation} - P_{measurement})^2}{N}} \quad (13)$$

where $P_{calculation}$– dust concentration is calculated by the formula; $P_{measurement}$– measured observed dust content value; N– number of samples.

4. Results

Based on equation (12), a survey, correlation analysis, and regression analysis of PM2.5 calculation models with Landsat 8 OLI images taken on June 6, 2019, were carried out.

In studies to determine the concentration of fine PM2.5 particles by similarity with the aerosol optical thickness (AOT) according to Landsat satellite images, blue, green, and red wavelengths in the range of 0.45–0.69 μm are mainly used (Othman et al., 2010). Therefore, in this study, four spectral channels of the Landsat 8 OLI image were used to obtain dust scattering schemes: channel 1 – Coastal aerosol (0.43–0.45 μm), channel 2 - Blue (0.45–0.51 μm), channel 3 - Green (0.53–0.60 μm) and channel 4 - Red (0.63–0.68 μm).

Based on the initial image data, processing steps were performed to extract data from the image; then, they were combined with ground-based measurement data to calculate the coefficient of the linear regression equation (see Table 5). A linear regression analysis was performed based on dust concentrations from 10 weather stations (see Tables 4.1 and 4.2).

Regression models were calculated and analyzed using Microsoft Excel software. The value of the atmospheric reflection coefficient Ri is considered an independent variable. The dust concentration PM2.5 measured at ground stations is a dependent variable. The results of the regression calculation are shown in Table 6.1 and Table 6.2.

It can be seen from the analysis results (Table 6.1) that when using independent spectral channels, the correlation coefficient R is very low. Combining spectral channels gives better results. The calculation results show that when combining the atmospheric reflection coefficient calculated using four spectral channels, the highest correlation coefficient is observed (R = 0.9143 and R2 = 0.8361).

It can be seen from the analysis results (Table 6.2) that when using independent spectral channels, the correlation coefficient R is very low. Combining spectral channels gives better results. The calculation results

Table 5
Model of regression and correlation analysis.

		Channel 1	Channel 2	Channel 3	Channel 4
$PM_{2,5}$=	a_0	$+a_1.R_1$			
$PM_{2,5}$=	a_0		$+a_2.R_2$		
$PM_{2,5}$=	a_0			$+a_3.R_3$	$+a_4.R_4$
$PM_{2,5}$=	a_0	$+a_1.R_1$	$+a_2.R_2$		
$PM_{2,5}$=	a_0	$+a_1.R_1$		$+a_3.R_3$	
$PM_{2,5}$=	a_0	$+a_1.R_1$			$+a_4.R_4$
$PM_{2,5}$=	a_0		$+a_2.R_2$	$+a_3.R_3$	
$PM_{2,5}$=	a_0		$+a_2.R_2$		$+a_4.R_4$
$PM_{2,5}$=	a_0			$+a_3.R_3$	$+a_4.R_4$
$PM_{2,5}$=	a_0	$+a_1.R_1$	$+a_2.R_2$	$+a_3.R_3$	
$PM_{2,5}$=	a_0	$+a_1.R_1$	$+a_2.R_2$		$+a_4.R_4$
$PM_{2,5}$=	a_0	$+a_1.R_1$		$+a_3.R_3$	$+a_4.R_4$
$PM_{2,5}$=	a_0		$+a_2.R_2$	$+a_3.R_3$	$+a_4.R_4$
$PM_{2,5}$=	a_0	$+a_1.R_1$	$+a_2.R_2$	$+a_3.R_3$	

Table 6.1
Results of correlation and regression analysis.

a_0	a_1	a_2	a_3	a_4	R	R^2	RMSE (μg / m^3)
0,00160	−0,0041				0,1452	0,0211	0,38,493
0,0030		−0,0008			0,04	0,0016	0,13,738
0,0036			0,0014		0,0707	0,0050	0,32,818
0,0035				0,0010	0,0655	0,0043	0,32,161
−0,0145	−0,0614	0,0437			0,4778	0,2283	0,51,726
−0,0021	−0,0325		0,0218		0,4923	0,2424	0,70,960
−0,0006	−0,0175			0,0090	0,3546	0,1258	0,70,251
0,0053		−0,0121	0,0116		0,2535	0,0643	0,46,113
0,0043		0,0099		0,0076	0,2242	0,0503	0,45,484
0,0036			0,0014	−0,00004	0,0707	0,0050	0,65,045
−0,0143	−0,0730	0,0348	0,0177		0,6053	0,3664	0,84,201
−0,0142	−0,0606	0,0425		0,0005	0,4780	0,2285	0,83,516
−0,0020	−0,0334		0,0264	−0,0035	0,4983	0,2484	102,740
0,0053		−0,0131	0,0086	0,0033	0,2632	0,0693	0,77,930
−0,0496	−0,20,733	0,13,929	0,08063	−0,0572	0,9143	0,8361	0,37,376

Table 6.2
Results of correlation and regression analysis.

a_0	a_1	a_2	a_3	a_4	R	R^2	RMSE (μg / m^3)
0,00336	−0,00978				0,0405	0,0016	0,84,919
0,0050		−0,0081			0,0392	0,0784	0,81,017
0,0027			−0,0121		0,0854	0,0072	0,73,311
0,0042				−0,0103	0,0983	0,0096	0,71,752
0,0007	−0,0263	0,0141			0,0413	0,0017	164,778
0,0173	0,0610		−0,0628		0,1874	0,0351	157,067
0,0298	0,0674			−0,0542	0,2382	0,0567	155,494
0,0082		0,0599	−0,0709		0,2091	0,0437	153,169
0,0244		0,0796		−0,0718	0,3039	0,0923	151,601
0,0161			0,0697	−0,0648	0,1310	0,0171	143,901
0,0046	−0,0223	0,0787	−0,0708		0,2106	0,0443	236,927
0,0075	−0,1188	0,1901		−0,0798	0,3426	0,1173	235,353
0,0325	0,0636		0,0244	−0,0708	0,2418	0,0584	227,648
0,0311		0,0765	0,0438	−0,1037	0,3165	0,1001	223,754
0	−0,3143	0,3539	0,1501	−0,1972	0,9889	0,9779	309,266

show that when combining the atmospheric reflection coefficient calculated from 4 spectral channels, the highest correlation coefficient is observed ($R = 0.9889$ and R2 = 0.9779).

It is necessary to consider the value of the probability of significance (Sig. F) (Table 7.1), which should not be more than 0.05, in which case the model is considered significant. Thus, the equation used to map the concentration of fine PM2.5 particles for the city of Moscow is written as follows:

$$PM_{2,5} = -0,0496 - 0,20733R_1 + 0,13929R_2 + 0,08063R_3 - 0,0572R_4 \quad (14)$$

It is necessary to consider the value of the probability of significance (Sig. F) (tab. 7.2), which should be no more than 0.05 – then the model is significant. Thus, the equation used to map the concentration of fine PM2.5 particles for the city of Moscow is written as follows:

$$PM_{2,5} = -0,3143R_1 + 0,35394R_2 + 0,15012R_3 - 0,1973R_4 \quad (15)$$

Based on the formula (14), using the ArcGIS program, a map of the concentration of fine dust PM2.5 in the city of Moscow as of June 6, 2019, was done (Fig. 4).

Based on the formula (15), using the ArcGIS program, a map of the concentration of fine dust PM2.5 in the city of Moscow on December 10, 2020, was done (Fig. 5).

Table 7.1
ANOVA table.

ANOVA	*Df*	*SS*	*MS*	*F*	*Significance F*
Regression	4	468233E-06	1,17E-06	6,377,984	0,033593452
Remains	5	917674E-07	1,84E-07		
General	9	0,0000056			

Table 7.2
ANOVA table.

ANOVA	*Df*	*SS*	*MS*	*F*	*Significance F*
Regression	4	0,001345	0,00034	134,169	284625E-05
Remains	6	15039E-05	2,5E-06		
General	10	0,00136025			

The results of this study (R = 0.9143 and R2 = 0.8361 and the lowest average error RMSE = 0.37376 μm/m3) show that the method for determining air pollution with fine PM2.5 particles can be applied using various coefficients to increase the accuracy of the satellite image from Landsat 8 OLI in combination with data on PM2.5 concentrations obtained by local ground stations. Landsat 8 OLI images were successfully used to calculate the concentration of PM2.5 on the territory of Moscow. The resulting map of dust pollution by fine particles shows the concentrations of PM2.5 in the region of the city.

The values of the concentration of fine dust PM2.5 are compared with actual values - data on air pollution in the city with fine dust PM2.5. It, therefore, can be concluded that the concentration of PM2.5 (see Figs. 4, 5) reflects the actual values; PM2.5 pollution is concentrated in the center of Moscow and on the main transport highways.

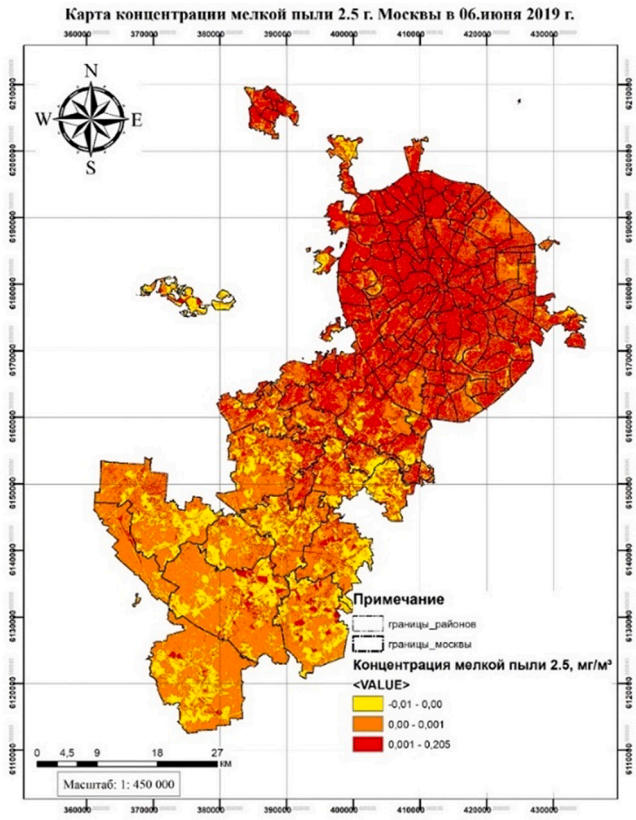

Fig. 4. Scheme of the concentration of fine dust PM2.5 in Moscow on June 6, 2019.

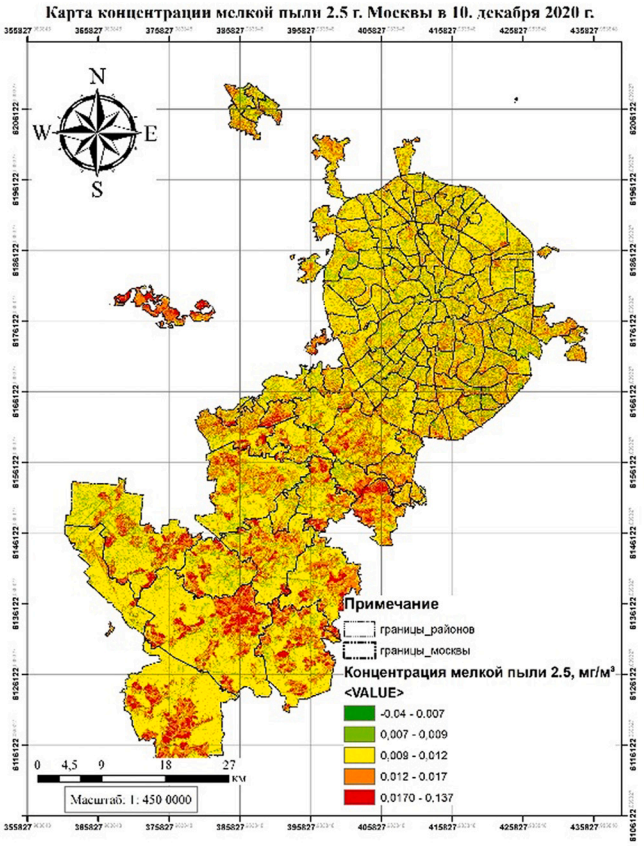

Fig. 5. The scheme of the concentration of fine dust PM2.5 in Moscow on December 10, 2020.

5. Discussion

5.1. The relationship between the urban heat island and the urban pollution island

The importance of studying the consequences of combining an urban heat island and an urban pollution island has been emphasized since 2004 (Crutzen, 2004). However, different reasons should separate the study of urban heat islands and urban pollution islands (Li et al., 2018). Recently, holistic approaches that allow conceptualizing double-action countermeasures have become increasingly widespread (Baklanov et al., 2016; Crutzen, 2004).

Assessing the relationship between urban heat islands and urban pollution island is a big task. Even though it is expensive, installing and maintaining a dense sensor network is necessary to study near-surface parameters. Alternatively, uncontrolled areas can be estimated using geostatistics based on a relatively small number of direct observations (Merbitz et al., 2012) or by applying complex algorithms to remotely obtained images (Nichol, 1996).

The probability of forming an urban heat island and an urban pollution island increases as we approach the city center and sources of heat/emissions, air stagnation, clear anticyclonic conditions, warm/hot seasons, night conditions, the size of the city, and population. Impacts of UHI and UPI affect climatological aspects such as sunlight, precipitation, temperature, and air quality. Under certain circumstances, the positive correlation between the urban heat island and the urban pollution island may change to the opposite due to the stimulation of vertical transport, mixing, and inversion violation. In addition, since the budgetary conditions for the formation and increase of an urban heat island and an urban pollution island are associated with advection mechanisms, a trend towards chemical production/losses, turbulence, dry or wet deposition, and anthropogenic emissions, the net movement may differ at night and during the day (Sarrat et al., 2006).

Due to a larger and longer-term middle layer, there may be a more severe deterioration in air quality in large cities. Urban winds are generated by urban heat islands and are characterized by converging flows on the surface to the city center. Based on observations and considering the current trend towards overcrowding of urban centers with fewer parking lots and wide traffic lanes, we should look for the problem of setting thresholds for dark airflow, at least on pedestrian streets (Krüger et al., 2011). In addition, stuck plumes of ozone precursors can spread further downwind, exposing suburban areas and nearby small towns to air quality degradation.

5.2. Future research

Based on the data obtained from satellite images of the city of Moscow on June 6, 2019, and December 10, 2019, using mathematical formulas that convert digital data, combined with data obtained at meteorological stations on Earth, the method of calculating multidimensional regression gave us reliable results that enable us to draw valid conclusions. As part of future research, more resources can be invested in increasing the density of fine dust pollution survey networks in the city of Moscow in a bid to improve the accuracy of the computational model. Finally, future research may include linking the results of determining polluted urban islands and urban thermal islands based on microclimate simulation models. Thus, special attention is paid to the factors of the urban heat island, which directly affect the distribution of fine dust in the city, to offer solutions for the simultaneous minimization of the urban heat island (UHI) and the urban pollution island (UPI).

6. Conclusion

Moscow - a European metropolis located in a temperate climate zone, has been selected for the research purpose. Identifying contaminated areas has been conducted with the support of ArcGIS software, converting satellite images of Landsat 8 OLI, measurement data at meteorological monitoring stations in Moscow within the framework of the CityAir project, and other spatial analysis tools. The results of this study ($R = 0.9143$ and $R2 = 0.8361$ and the lowest average error RMSE $= 0.37376$ μm/m3) show that the method for determining air pollution with fine PM2.5 particles can be applied using various coefficients to increase the accuracy of the satellite image from Landsat 8 OLI in combination with data on PM2.5 concentrations obtained by local ground stations.

According to the analysis of the obtained images, the air pollution zones are mainly concentrated in the center, in the north, and gradually decrease in the south-west of the city. A high population density may cause the observed phenomenon in the northern, the concentration of production, housing and transport communications, and private transportation contributes to the formation of PM2.5 particles. The following features characterize the high level of urbanization in Moscow: the proximity of buildings, which positively affects the comfort of the microclimate in the summer due to protection zones and shading of roads, and negatively - in the winter due to excessive shading. However, most infrastructural factors and the urbanization increase are responsible for air pollution. Based on the results obtained, it can be concluded that the advantage of using remote sensing technology is to establish the influence of the atmosphere and geological features of the Earth's surface on determining the concentration.

Urban heat islands and urban pollution islands manifest urban microclimatic transformations and thermochemical disturbances occurring in megacities. Studies have shown that high temperature, low relative humidity, low wind speed, and the absence of clouds simultaneously affect the development of an urban heat island and the heavy pollution of the territory.

In general, within the framework of the analysis of microclimatic conditions and the environmental situation in the city, it is difficult to find a universal formula for identifying the mutual influence of urban heat islands and pollution. Still, by combining the research results with new results from related disciplines, it is possible to compile a list of criteria for evaluating the effectiveness of urban design measures:

- For buildings and building surfaces: aerodynamically uneven urban profiles and radial street layouts should be encouraged to cause turbulent heat propagation between buildings and prevent stagnation of pollutants; appropriate blackout provisions should be provided to avoid unnecessary overheating of premises and limit the use of air conditioning systems; centralized large buildings and hotels should switch to heat recovery systems to recirculate the pumped hot air into hot water systems or secondary circuits; roofs and sidewalks with a high albedo should be preferred over traditional paradigms, but special legislation should contain recommendations regarding the potential disadvantages of UV radiation;
- For urban transport, restrictions should be introduced on certain types of transportation and special rules governing the number and type of vehicles in hotspots in different city areas. The use of hybrid cars and alternative fuels is one of the directions that allow getting away from traditional technologies of combustion of hydrocarbons in the internal combustion engine. Prospective studies establish the type of road surface, tires and brake linings, anti-icing agents of road surfaces that pollute objects located near roads;
- For water surfaces in the city: large bodies of water should be surrounded by low buildings so that the wind brings fewer heat flows to the city; an artificial cooling system, such as water spray systems, should be organized in the form of several small interventions designed taking into account the prevailing wind regimes and synergetic cooling;
- For urban green areas: parks should be added to the urban structure to stimulate local breezes and provide a higher volumetric heat capacity; the possibility of creating vertical green spaces and roof gardens should be considered, especially in high-rise buildings that are exposed to solar radiation for a long time to reduce the use of AC systems; vegetation cover in the form of overhanging vines or the likes, should shade large masses of asphalt and concrete; where possible, preference should be given to species with a low level of maintenance and a low potential for ozone formation.

Based on the results obtained, the influence of the atmosphere and geological features of the Earth's surface on the determination of PM2.5 dust from the Landsat 8 OLI satellite image is visible. Further research in studying image correction methods to improve the accuracy of the technique used in work will be a step in the right direction.

Declaration of Competing Interest

The authors declare no conflict of interest.

Acknowledgments

This project is supported by the Moscow State University of Civil Engineering.

References

Baklanov, A., Molina, L.T., Gauss, M., 2016. Megacities, air quality, and climate. In: Atmospheric Environment, vol. 126. Elsevier Ltd., pp. 235–249. https://doi.org/10.1016/j.atmosenv.2015.11.059

Bilal, M., Nazeer, M., Nichol, J.E., Bleiweiss, M.P., Qiu, Z., Jäkel, E., Campbell, J.R., Atique, L., Huang, X., Lolli, S., 2019. A simplified and robust surface reflectance estimation method (SREM) over diverse land surfaces using multi-sensor data. Remote Sens. 11 (11) https://doi.org/10.3390/rs11111344.

Chavez, P.S., 1996. Image-Based Atmospheric Corrections - Revisited and Improved. photogrammetric Engineering & Remote Sensing.

Crutzen, P.J., 2004. New directions: the growing urban heat and pollution “island” effect - impact on chemistry and climate. In: Atmospheric Environment, vol. 38. Elsevier Ltd, pp. 3539–3540. https://doi.org/10.1016/j.atmosenv.2004.03.032. Issue 21.

Dubovik, O., Holben, B., Eck, T.F., Smirnov, A., Kaufman, Y.J., King, M.D., Tanré, D., Slutsker, I., 2001. Variability of Absorption and Optical Properties of Key Aerosol Types Observed in Worldwide Locations. American Meteorological Society.

Elsayed, I.S.M., 2012. Mitigation of the urban heat island of the city of Kuala Lumpur, Malaysia. Middle East Journal of Scientific Research 11 (11), 1602–1613. https://doi.org/10.5829/idosi.mejsr.2012.11.11.1590.

Engel-Cox, J.A., Holloman, C.H., Coutant, B.W., Hoff, R.M., 2004. Qualitative and quantitative evaluation of MODIS satellite sensor data for regional and urban scale air quality. Atmos. Environ. 38 (16), 2495–2509. https://doi.org/10.1016/j.atmosenv.2004.01.039.

Hutchison, K.D., Smith, S., Faruqui, S.J., 2005. Correlating MODIS aerosol optical thickness data with ground-based PM 2.5 observations across Texas for use in a real-time air quality prediction system. Atmos. Environ. 39 (37), 7190–7203. https://doi.org/10.1016/j.atmosenv.2005.08.036.

Kaufman, Y.J., Tanré, D., Gordon, H.R., Nakajima, T., Lenoble, J., Frouin, R., Grassl, H., Herman, B.M., King, M.D., Teillet, P.M., 1997. Passive remote sensing of tropospheric aerosol and atmospheric correction for the aerosol effect. Journal of Geophysical Research Atmospheres 102 (14), 16815–16830. https://doi.org/10.1029/97jd01496.

Landsat 8 (L8), 2019. Data Users Handbook..

Li, H., Meier, F., Lee, X., Chakraborty, T., Liu, J., Schaap, M., Sodoudi, S., 2018. Interaction between urban heat island and urban pollution island during summer in Berlin. Sci. Total Environ. 636, 818–828. https://doi.org/10.1016/j.scitotenv.2018.04.254.

Liaw, J.J., Huang, Y.F., Hsieh, C.H., Lin, D.C., Luo, C.H., 2020. PM2.5 concentration estimation based on image processing schemes and simple linear regression. Sensors (Switzerland) 20 (8). https://doi.org/10.3390/s20082423.

Liu, Y., Paciorek, C.J., Koutrakis, P., 2009. Estimating regional spatial and temporal variability of PM2.5 concentrations using satellite data, meteorology, and land use information. Environ. Health Perspect. 117 (6), 886–892. https://doi.org/10.1289/ehp.0800123.

Melstrom, P., Koszowski, B., Thanner, M.H., Hoh, E., King, B., Bunnell, R., McAfee, T., 2017. Measuring PM2.5, ultrafine particles, nicotine air and wipe samples following the use of electronic cigarettes. Nicotine and Tobacco Research 19 (9), 1055–1061. https://doi.org/10.1093/ntr/ntx058.

Merbitz, H., Buttstädt, M., Michael, S., Dott, W., Schneider, C., 2012. GIS-based identification of spatial variables enhancing heat and poor air quality in urban areas. Appl. Geogr. 33 (1), 94–106. https://doi.org/10.1016/j.apgeog.2011.06.008.

Nichol, J.E., 1996. Planning and Design, vol. 23.

Othman, N., Zubir, M., Jafri, M., Lim, San, H., 2010. Estimating particulate matter concentration over arid region using satellite remote sensing: a case study in Makkah, Saudi Arabia. Mod. Appl. Sci. 4 (11). www.ccsenet.org/mas.

Paciorek, C.J., Liu, Y., 2009. Limitations of remotely sensed aerosol as a spatial proxy for fine particulate matter. Environ. Health Perspect. 117 (6), 904–909. https://doi.org/10.1289/ehp.0800360.

Raaschou-Nielsen, O., Andersen, Z.J., Beelen, R., Samoli, E., Stafoggia, M., Weinmayr, G., Hoffmann, B., Fischer, P., Nieuwenhuijsen, M.J., Brunekreef, B., Xun, W.W., Katsouyanni, K., Dimakopoulou, K., Sommar, J., Forsberg, B., Modig, L., Oudin, A., Oftedal, B., Schwarze, P.E., Hoek, G., 2013. Air pollution and lung cancer incidence in 17 European cohorts: Prospective analyses from the European Study of Cohorts for Air Pollution Effects (ESCAPE). Lancet Oncol. 14 (9), 813–822. https://doi.org/10.1016/S1470-2045(13)70279–1.

Sarrat, C., Lemonsu, A., Masson, V., Guedalia, D., 2006. Impact of urban heat island on regional atmospheric pollution. Atmos. Environ. 40 (10), 1743–1758. https://doi.org/10.1016/j.atmosenv.2005.11.037.

Shi, W., Wong, M.S., Wang, J., Zhao, Y., 2012. Analysis of airborne particulate matter (PM2.5) over Hong Kong using remote sensing and GIS. Sensors (Switzerland) 12 (6), 6825–6836. https://doi.org/10.3390/s120606825.

Sobrino, J.A., Jiménez-Muñoz, J.C., Paolini, L., 2004. Land surface temperature retrieval from LANDSAT TM 5. Remote Sens. Environ. 90 (4), 434–440. https://doi.org/10.1016/j.rse.2004.02.003.

Somvanshi, S.S., Vashisht, A., Chandra, U., Kaushik, G., 2019. Delhi air pollution modeling using remote sensing technique. In: Handbook of Environmental Materials Management. Springer International Publishing, pp. 1–27. https://doi.org/10.1007/978-3-319-58538-3_174-1.

Susan Moran, M., Jackson, R.D., Slater, P.N., TeiUet, P.M., 1992. Evaluation of Simplified Procedures for Retrieval of Land Surface Reflectance Factors from Satellite Sensor Output, Vol. 41.

Vailshery, L.S., Jaganmohan, M., Nagendra, H., 2013. Effect of street trees on microclimate and air pollution in a tropical city. Urban Forestry and Urban Greening 12 (3), 408–415. https://doi.org/10.1016/j.ufug.2013.03.002.

Wang, J., Christopher, S.A., 2003. Intercomparison between satellite-derived aerosol optical thickness and PM2.5 mass: implications for air quality studies. Geophys. Res. Lett. 30 (21) https://doi.org/10.1029/2003GL018174.

Zhang, Y., Li, Z., 2015. Remote sensing of atmospheric fine particulate matter (PM2.5) mass concentration near the ground from satellite observation. Remote Sens. Environ. 160, 252–262. https://doi.org/10.1016/j.rse.2015.02.005.